Construction and Building Materials 367 (2023) 130024

Contents lists available at ScienceDirect

Construction and Building Materials

journal homepage: www.elsevier.com/locate/conbuildmat

Design of a smart lime mortar with conductive micro and nano fillers for structural health monitoring

Anastasios Drougkas [a,b,*], Vasilis Sarhosis [a], Muhammed Basheer [a], Antonella D'Alessandro [c], Filippo Ubertini [c]

[a] School of Civil Engineering, University of Leeds, Woodhouse Lane, LS2 9JT Leeds, United Kingdom
[b] Serra Húnter Fellow, Department of Strength of Materials and Structural Engineering, Universitat Politècnica de Catalunya (UPC-BarcelonaTech), C/Colom 11, 08222 Terrassa, Spain
[c] Department of Civil and Environmental Engineering, University of Perugia, Via G. Duranti 93, 06125 Perugia, Italy

ARTICLE INFO

Keywords:
Lime mortar
Carbon nanotubes
Carbon microfibers
Graphite
Smart materials
Structural health monitoring

ABSTRACT

Structural health monitoring is an essential tool for assessing the performance of buildings and infrastructure, especially after critical events or the application of structural interventions. When dealing with architectural heritage structures, both structural health monitoring instrumentation and intervention materials need to be as inconspicuous and unintrusive as possible, both in terms of mechanical compatibility and aesthetics. Therefore, the design of smart sensors based on construction materials used in conservation engineering promises to provide an acceptable integrated structural health monitoring and upgrading solution for historic structures. In this paper an experimental investigation of smart intervention materials for historic masonry structures is presented. The materials consisted of natural hydraulic lime mortars modified through the inclusion of electrically conductive micro- and nanofillers: graphite, carbon nanotubes and carbon microfibres. The fillers provide multifunctionality to the matrix material based on an enhancement of its piezoresistive characteristics. Further, they result in an improvement of the mechanical properties of the intervention material without compromising its mechanical and chemical compatibility with the original structure. The resulting materials were evaluated based on mechanical property improvement, piezoresistivity enhancement and ease of production.

1. Introduction

The mechanical and chemical properties of masonry mortars have been the subject of extensive study in the literature, especially for mortars containing both lime and cement. While lime mortars with no cement content have received special attention in the literature, mostly in a conservation context [1,3,28], comprehensive studies on mechanical characterisation [17,27,31] and structural applications [14,35,40] remain limited in number and scope. This is potentially due to protracted curing times compared to cement or lime-cement mortars, as well as reduced strength and durability of the material. Nevertheless, investigations on lime mortar are motivated by its nearly ubiquitous presence in historic buildings as well as its use as a widely acceptable intervention material, both as a repointing agent or in reconstructed segments, in architectural heritage structures [25,24].

Central to conservation engineering practice is the concept of structural health monitoring (SHM), which is the automated assessment of the condition and performance of structures through continuous measurements of features such as temperature and deformations [37]. The performance and durability of structural interventions in architectural heritage structures need to be monitored to assess the compatibility of new and existing materials, as well as for measuring the overall improvement of the structures' condition following intervention. SHM is typically performed through the use of externally mounted, complex and expensive instrumentation [22,38], which can be aesthetically or functionally burdening to the original texture of the structure.

Multifunctional materials offer a promising workaround to several practical limitations associated with SHM, especially in terms of their application to architectural heritage structures. Multifunctionality in structural materials includes self-sensing capabilities through piezoresistivity, namely the physical and constitutive relation between mechanical strain and electrical resistivity [19,39]. Enhanced piezoresistivity in cementitious materials, such as concrete and mortar, can be achieved through modification of the mix design using

* Corresponding author at: School of Civil Engineering, University of Leeds, Woodhouse Lane, LS2 9JT Leeds, United Kingdom.
E-mail addresses: A.Drougkas@leeds.ac.uk, anastasios.drougkas@upc.edu (A. Drougkas).

https://doi.org/10.1016/j.conbuildmat.2022.130024
Received 4 April 2022; Received in revised form 7 December 2022; Accepted 9 December 2022
Available online 12 January 2023
0950-0618/© 2023 The Authors. Published by Elsevier Ltd. This is an open access article under the CC BY license (http://creativecommons.org/licenses/by/4.0/).

conductive carbon-based micro and nanofillers [32], while the inclusion of even nonconductive high aspect ratio fibres has been shown to enhance the piezoresistivity of cementitious composites doped with conductive powder [13,18]. Cementitious smart materials, created by dispersing nanofillers in an aqueous solution before mixing it with the binder and aggregates, pose a practical challenge due to their predisposition to create nanofiller agglomerations during mixing, necessitating the use of tailored dispersion and mixing procedures. In this way, it is possible to reliably enhance and stabilise their sensing and mechanical properties, enhance nanofiller efficiency and decrease mechanical energy required for mixing. Regardless, cementitious materials are highly suitable for nanomodification due to featuring material components, pores and cracks at the micro- and nano-scale. Applications of such smart materials have generally demonstrated significantly enhanced piezoresistivity combined with substantially improved mechanical performance as a function of the amount of micro and nanofillers incorporated in the mix [2]. However, although nanomodification of lime mortars has been previously attempted for enhancing mechanical performance [15], extensive piezoresistive studies for lime mortars have not been so far elaborated.

The design of a smart lime mortar, modified using conductive micro and nanofillers for enhanced piezoresistivity and mechanical properties, is an important step towards the development of smart intervention materials for SHM in historic masonry buildings, with improved strength and durability and a high degree of compatibility with *in situ* materials. This paper describes the design and experimental testing of this smart lime mortar, through extensive mechanical and electrical characterisation.

Firstly, the constituent materials of the smart mortar used in this investigation are presented, along with the properties determined experimentally. Next, the experimental programme, including the preparation and testing procedures for the smart mortar specimens, is presented in detail. Subsequently, the experimental results are presented and discussed, illustrating the effect of different filler content on the properties of the smart mortar. The paper is concluded with a summary of the findings and recommendations for future work.

2. Experimental programme

2.1. Materials

The base material in this investigation was lime mortar, composed of a lime-based binder and a fine aggregate. The binder in this mortar was natural hydraulic lime (NHL) conforming to EN 459-1 standard [7]. A class of NHL 3.5 (moderately hydraulic) was selected for this investigation, this being a typical choice for building conservation and repointing projects [29]. NHL is produced by firing and slaking clay limestone or siliceous limestone, its mineral phases being primarily dicalcium silicate and calcium hydroxide [41]. Hardening of NHL primarily consists of a hydraulic component arising through a hydration reaction with water, forming calcium silicate hydrate. This reaction follows the formula:

$$2(2CaO{\cdot}SiO_2) + 4H_2O \rightarrow 3CaO{\cdot}2SiO_2{\cdot}3H_2O + Ca(OH)_2 \quad (1)$$

Following contact with water, a secondary aerial component is activated, leading to the formation of calcium carbonate crystals by the reaction of calcium hydroxide with carbon dioxide in the air according to the reaction formula:

$$Ca(OH)_2 + CO_2 + nH_2O \rightarrow CaCO_3 + (n+1)H_2O \quad (2)$$

The aggregate used in this investigation was a siliceous sand with a nominal grain size distribution of 0–3 mm, suitable for the construction of masonry mortar. For determining the granulometry of the sand, EN 196–1 standard was consulted [5]. The sand samples were dried at 110 ^{0}C to constant mass, achieved when the hourly change of mass was less than 0.01 %. The sand sample was subsequently passed through stacked sieves placed in a mechanical shaker for 10 min. Two different samples of sand were tested, one weighing 200 g and one weighing 400 g, both returning very similar results. The mean results of the two sieve analyses are tabulated in Table 1 and illustrated in Fig. 1. During the drying process, the initial moisture content of the sand was determined to be 2.58 %.

Table 1
Sieve analysis results for siliceous sand.

Sieve aperture (mm)	Weight retained (%)	Cumulative weight retained (%)	Weight passing (%)
4	0.30	0.30	99.7
2	19.73	20.02	79.30
1	26.03	46.04	53.40
0.5	17.58	63.62	35.58
0.25	13.10	76.72	20.70
0.125	8.22	84.94	12.59
0.063	13.69	98.63	0.91
Tray	1.37	100.00	0.00

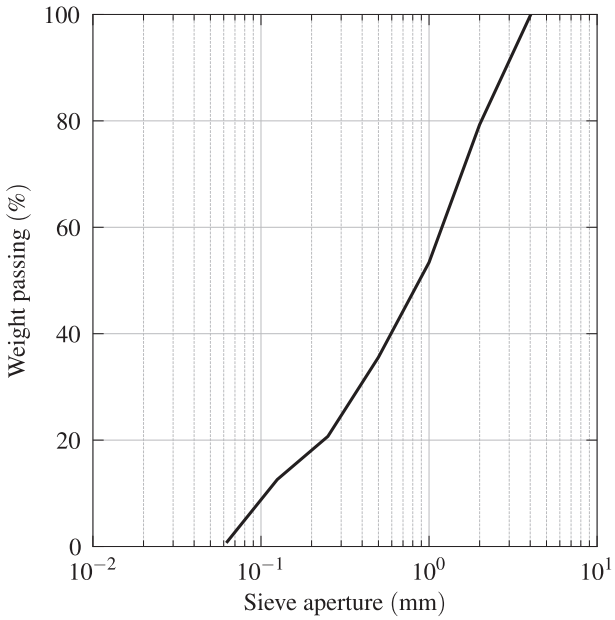

Fig. 1. Graph of sieve analysis results for siliceous sand.

The mixing of the mortar was performed according to EN 196-1 standard [5]. While this standard specifies that the binder and aggregate be proportioned by weight, the mix proportions of the dry components were 1 part binder to 3 parts aggregate by volume, as suggested by masonry construction practice. This results in a less binder-rich mortar compared to the one prescribed by the standard, which is, nevertheless, suitable as a repointing agent in conservation projects. No other additives, such as plasticisers, were incorporated in the mortar mixes.

Optimal water content in lime mortars can vary widely depending on the targeted flow value, ambient temperature and humidity during casting, moisture content of the sand and envisaged structural application [17,31,34]. In industrial practice for masonry construction and repointing mortar, water/binder (w/b) is adjusted on-site through gradual addition of water during mixing until the empirically required mortar consistency is obtained [16]. In the present investigation, aqueous solutions of conductive fillers were prepared on fixed volumes of water, requiring a predetermined amount of water to be used for each casting. Therefore, test batches of mortar were prepared with varying water content for assessing the workability of the mortar. To maintain

Table 2
Bulk densities of base mortar components.

Component	ρ_b (kg/m^3)
NHL	667
Sand	1420
Water	998

Table 3
Physical and geometrical properties of fillers: bulk density, electrical resistivity and aspect ratio.

Filler	ρ_b (kg/m^3)	ρ (Ω•cm)	a (−)
G	1200	3.0–5.0 × 10^{-4}	~12
CMF	390	1.5 × 10^{-3}	~900
CNT	50–150	1.0 × 10^{-5}	~600–700

uniformity between mixes, the sand was stored in hermetically sealed containers for maintaining a constant moisture content. The bulk densities, ρ_b, of the base materials are presented in Table 2.

Three types of fillers were incorporated in the tested mortar mixes: graphite powder (G), carbon microfibers (CMFs) and carbon nanotubes (CNTs). G is an allotrope of carbon, shaped in oblate 3D particles with low aspect ratios, which, nevertheless, can impart high electrical conductivity to cementitious matrices, albeit at high levels of doping [9]. The CMFs used in this study were produced from precision cutting of continuous carbon fibre tows into pieces of 6 mm length, with each individual strand having a diameter of 7 μm. The sizing agent of the CMFs was glycerine, which is suitable for water-based systems (SIGRAFIL Short Carbon Fibres). CNTs are fibrous fillers consisting of carbon atom lattices forming single cylinders or multiple nested cylinders held together by van der Waals forces. They have diameters in the range of a few nanometres and have very high aspect ratios. In the present investigation, multi walled rather than single walled CNTs were used (Arkema Multi-Walled Graphistrength C-100). Multi walled CNTs consist of concentric cylinders of graphene layers which can enhance the electrical properties of the materials in which they are dispersed [11]. The bulk density, ρ_b, electrical resistivity, ρ, and aspect ratio, a, of the used fillers are presented in Table 3.

The different fillers were incorporated in varying proportions as a percentage of the binder by weight. G was incorporated in proportions ranging from 1 % to 20 % of the binder, while CMFs were incorporated in content ranging from 0.01 % to 0.2 %. CNTs were tested in concentrations between 0.1 % and 0.4 % of the binder. The different types of fillers may be used in applications at different scales, with CNTs being employed in targeted small-scale applications, sonication of large volumes of water being impractical, and with G and CMFs being capable of upscaling to larger volumes of material due to the low cost of the filler and the ease of achieving good dispersion with ordinary mechanical means.

CNTs were dispersed in the water used for each mix through ultrasonic homogenisation. The sonication cycle for each dispersion consisted of three 10-minute sonication periods, separated by 1-minute breaks, at 225 W processing power and 20 kHz frequency. No chemical dispersants were used in order not to disrupt the filler-binder interface and consequently affect the electrical conductivity of the hardened mortar. While it has been demonstrated that certain chemical dispersants can improve the piezoresistivity of cementitious composites, others can affect the filler-binder interface and potentially reduce conductivity [10,26]. Therefore, and with the added goal of minimising the inclusion of chemicals in the mortar mixes, no further dispersants were incorporated. G and CMFs were incorporated directly into the dry ingredients of the mortar (lime and sand) and mechanically mixed. This mechanical mixing process has been proven sufficient for evenly dispersing the G particles and CMF [2].

The mortar mixing process was as follows:

Table 4
List of produced mortar mixes with filler content.

Name	G/b (g/g%)	CMF/b (g/g%)	CNT/b (g/g%)
G0F0T0	0.0	0.0	0.0
G1F0T0	1.0	0.0	0.0
G2F0T0	2.5	0.0	0.0
G3F0T0	5.0	0.0	0.0
G4F0T0	10.0	0.0	0.0
G5F0T0	20.0	0.0	0.0
G0F1T0	0.0	0.01	0.0
G0F2T0	0.0	0.05	0.0
G0F3T0	0.0	0.10	0.0
G0F4T0	0.0	0.20	0.0
G0F0T1	0.0	0.0	0.1
G0F0T2	0.0	0.0	0.2
G0F0T3	0.0	0.0	0.3
G0F0T4	0.0	0.0	0.4

Table 5
Flow table spread-diameter results for unmodified mortar with varying water/binder.

w/b (g/g)	D (mm)
1.30	111.5
1.40	120.0
1.50	135.5
1.60	165.0
2.08	216.0

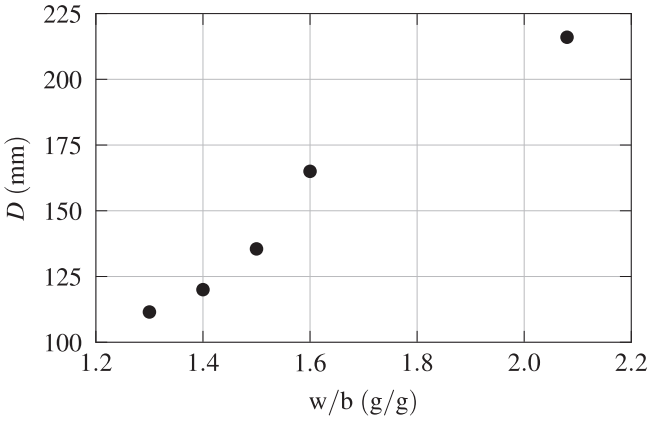

Fig. 2. Flow table spread-diameter results for unmodified lime mortar test batches.

a) all the lime was incorporated to half the sand in the mixer bowl and stirred for 5 min
b) the remaining sand was added to the mixer bowl and stirred for another 5 min
c) the water was added gradually over 10 min while mixing continuously

The fresh mortar was subsequently poured into steel moulds, compacted with a tamper rod and hermetically sealed in polyethylene bags for 7 days to prevent moisture loss while being kept in laboratory conditions (temperature 20 ± 2 ^{0}C). At the age of 4-days when the mortar cubes were sufficiently hardened, they were carefully demoulded and left to cure in the laboratory at an ambient relative humidity of 65 (±5) %. They remained there until tested, protected from draughts and direct sunlight. A list of the produced mortar mixes, with the content in G, CMFs and CNTs as a percentage of the binder by weight (G/b, CMF/b and CNT/b respectively) is shown in Table 4. In addition, a single batch of NHL paste without aggregates was produced for electromechanical testing.

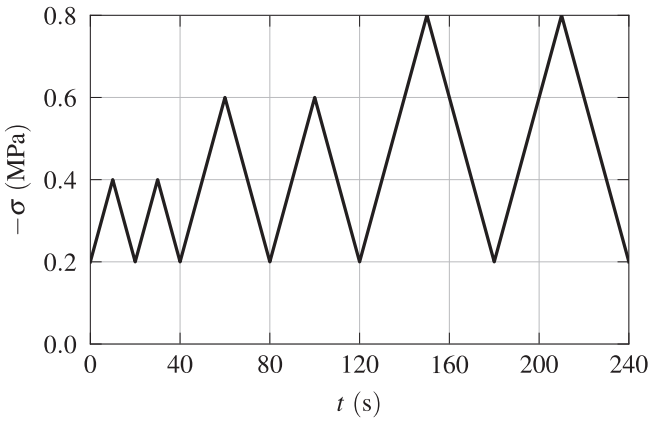

Fig. 3. Repeated compression load pattern for electromechanical testing of mortar cubes.

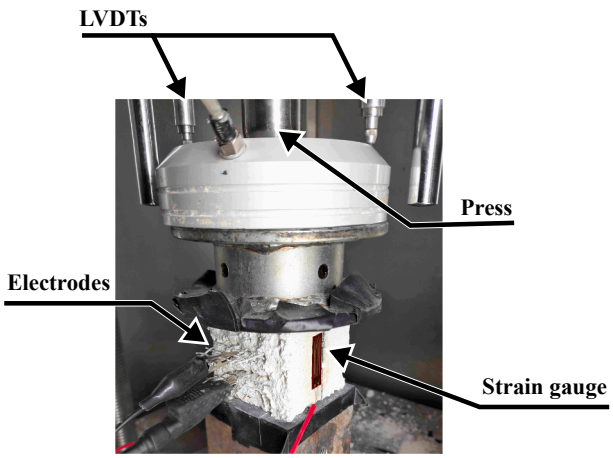

Fig. 4. Test setup and deformation sensor layout for electromechanical testing.

2.2. Testing programme

An experimental program was designed in order to characterize the physical, mechanical and electro-mechanical response of the above presented composite lime mortars. Experiments were carried out at the Materials Testing Laboratory of the University of Perugia. Flow table testing of the fresh mortar was conducted according to EN 459–2 standard [8]. The results of the preliminary batch flow table tests in terms of flow table spread in diameter, D, against w/b are tabulated in Table 5 and illustrated in Fig. 2. Based on these results and anticipating a potential decrease in the flow of the mortar with addition of the fillers, which could impact both the mixing process and the embedment of the mesh electrodes in the fresh mortar samples, the target flow value for the unmodified lime mortars was 150 mm, leading to the adoption of w/b = 1.60. For the NHL paste specimens, w/b was 0.6.

Mechanical testing of the mortar was performed on prisms sized 160 × 40 × 40 mm^3. The mortar prisms were tested in three-point bending for the determination of the flexural strength, f_b, the two resulting halves being tested in compression for determining the compressive strength, f_c, according to EN 1015–11 standard [6]. Additionally, LVDTs were employed during the compression tests for the determination of the Young's modulus, E. These tests were performed at the age of 49 days, allowing for sufficient hardening of the mortar through both hydraulic curing and carbonation to take place [17]. This extended curing period additionally allows for water loss to take place in the specimens in order to reduce the effect of moisture on conductivity. These tests were aimed at determining the enhancement of the strength of the mortars following modification. The force was applied at a rate of 10 N/s during the bending tests and at a rate of 50 N/s for the compressive tests, values which correspond to the lowest loading rates prescribed by the testing Standard.

Electrical resistivity tests were performed on cubes of size 50 × 50 × 50 mm^3. The development of the electrical resistivity during curing was monitored as part of a percolation study of the fillers in the material. The development of the density of the cubes during the curing period was also measured. Additionally, on the same day of mechanical testing of the prism, electromechanical testing of the cubes was performed for assessing the piezoresistivity of the various mixes. The cubes were subjected to repeated compression of increasing magnitude while monitoring the changes in the electrical resistivity. A sawtooth compressive loading pattern was applied to the specimens, with two repetitions each at 0.4, 0.6 and 0.8 MPa target stress from a minimum base stress of 0.2 MPa. The force was applied at a rate of 50 N/s during loading and unloading, same as for the standard compression tests. The repeated load pattern in terms of stress, σ, vs time, t, is illustrated in Fig. 3. All forces during the mechanical and electromechanical tests were applied using a UTM 14P testing machine by IPC Global.

Measurements of the deformation of the specimens under compression were mainly registered through two strain gauges attached along the loading direction. Lime mortar specimens can start cracking and spalling at very low loads, which could potentially render strain gauge readings inaccurate. Therefore, these measurements were complemented by measurements acquired from LVDTs mounted on the load plates. While this placement of the LVDTs meant that any deformation of the load plates and the interfacial adjustment between the load plates and the specimen were included in the measurement, the load cell deformation was determined separately and discounted from the measurements. Therefore, the low expected Young's modulus of the mortar entails that nearly all of the deformation of the entire setup occurs at the specimen. The test setup and instrumentation are shown in Fig. 4.

Electrical resistance measurements during the percolation study and during the electromechanical tests were acquired through woven stainless steel mesh electrodes embedded in the cubes. The resistivity, ρ, of the material of a specimen as measured through two-probe testing was calculated according to Ohm's second law:

$$\rho = R\frac{A}{L} \tag{3}$$

where A is the cross-sectional area of the specimen in the plane perpendicular to the measurement direction, L is the distance between the probes along the measurement direction and R is the measured resistance of the specimen. A schematic of the arrangement of the electrodes in the specimens is shown in Fig. 5. The lateral wires of the meshes were removed from the embedded part of the electrode to avoid physical interference with the fresh mortar during insertion.

A schematic of the electrical circuit used for conducting electrical measurements is shown in Fig. 6. A biphasic square wave voltage of ± 2 V with a 50 % duty cycle at 1 Hz frequency was supplied from a Rigol DG1022 function generator to eliminate signal drift due to polarisation [2]. Measurements of the electrical current, I, were acquired and logged using an NI PXIe-4071 digital multimeter and subsequently used to derive the resistance, R, from Ohm's first law:

$$R = \frac{V}{I} \tag{4}$$

The gauge factor, λ, for each produced specimen, indicating the magnitude of the piezoresistive effect during mechanical loading, was determined from the equation:

$$\lambda = (1+2\nu) + \frac{\Delta\rho/\rho}{\varepsilon} \tag{5}$$

where ν is the Poisson's ratio of the material and ε is the axial strain. This gauge factor was calculated through regression modelling of the

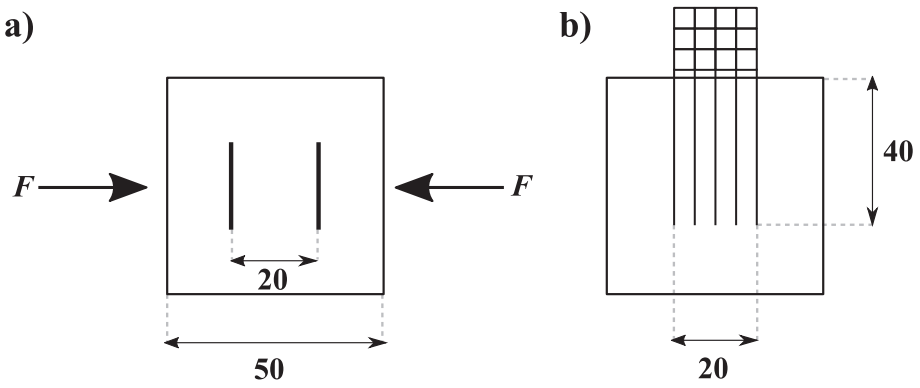

Fig. 5. Schematic of electromechanical measurement setup for cubic specimens: a) arrangement of embedded mesh electrodes with respect to loading force *F*. b) Cross section of specimen showing embedded mesh electrode. Dimensions in mm.

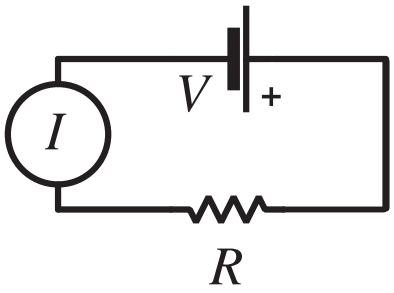

Fig. 6. Circuit diagram for electrical measurements: *R* is the resistance of the specimen, *V* is the voltage provided by the function generator and *I* is the current measured by the multimeter.

relationship between observed resistivity and strain during mechanical loading. A higher gauge factor, λ indicates higher sensitivity of the material's electrical resistivity to applied axial strain. The optimisation of the piezoresistive effect is typically achieved near the percolation threshold. In the case of these piezoresistive cementitious materials, where λ was expected to be in the order of magnitude of 100, the term in parentheses can be neglected. The sensing linearity, δ, equal to the 95 % confidence interval in the strain domain for the predicted linear regression, expresses the maximum deviation of the output of any sensor from the linear regression line of the sensor's output (resistivity) versus the input parameter being sensed (strain). Higher λ and lower δ values indicate improved sensitivity and linearity of the smart sensor respectively.

The open porosity of the mortar mixes was evaluated on 40 × 40 × 40 mm^3 cubic specimens. These specimens were cured for 49 days in lab conditions and subsequently conditioned in a thermal chamber at 70 ^{0}C and 10 % relative humidity until the daily change of weight was less than 0.1 % for obtaining the dry mass, m_d. The specimens achieved weight stability after 3 days of conditioning. Subsequently, the specimens were placed in a desiccator for 8 h in vacuum conditions. Finally, the specimens were submerged in demineralised water for 24 h for obtaining the saturated mass, m_s. Submerging the saturated specimen in water using a fine steel mesh and measuring the change in mass in the container holding the water yields the hydrostatic mass, m_h. Through the values for the dry mass, m_d, saturated mass, m_s and hydrostatic mass, m_h, of each specimen, it is possible to calculate the open porosity, φ, of the material through the equation:

$$\varphi = \frac{m_s - m_d}{m_s - m_h} \tag{6}$$

The internal structure of the composites, the dispersion of the carbon fillers within the matrix, and the homogeneity of the materials have been investigated through Scanning Electron Microscopy (SEM)

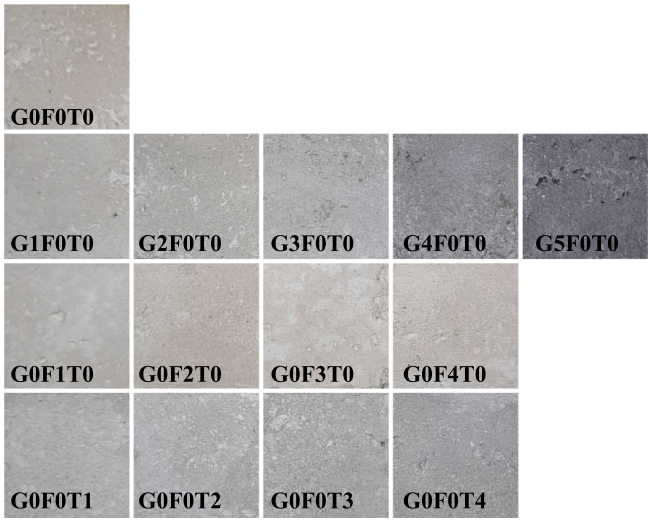

Fig. 7. Visual comparison of mortar mix colours.

micrographs. A fragment of unmodified lime mortar and lime paste, together with fragments of lime mortar doped with G, CNT and CMF were inspected by a field emission FESEM Supra 25-Zeiss, at different magnification levels.

3. Results and discussion

A qualitative visual comparison of the colour of the resulting mortar mixes is presented in Fig. 7. In the case of G, noticeable darkening of the mortar was obtained even for 1 % content. In the case of CMF, the colour of the mortar is not particularly affected by the filler even for the maximum content of 0.4 % used. Finally, in the case of CNT, slight darkening was noted for all doping levels. The lack of colour alteration for the CMF filler is advantageous compared to the other filler types from a conservation engineering perspective.

All the physical and mechanical properties of the mortar mixes from this research are summarised in Table 6, with percentile differences between unmodified and modified mortars indicated in parentheses.

Workability expressed through the flow, *D*, in the flow table test was not heavily affected by any of the filler types. The mortar mixes with filler exhibited higher workability than the unmodified mortar possibly due to slightly different temperature conditions during casting. However, among the mixes with the same filler type, increase in the filler content resulted in a decrease in *D*. The inclusion of a large volume percentage of sand in the mortar, coupled with high w/b, resulted in only a minor decrease in workability for increasing filler content.

Table 6
Physical and mechanical properties of mortar mixes at the age of 49 days (Percentile difference from the unmodified mortar G0F0T0 in parentheses).

Name	D(mm)	ρ_b(kg/m^3)	φ(%)	f_b(MPa)	f_c(MPa)	E(MPa)
G0F0T0	155	1625	27.42	0.466	1.179	841
G1F0T0	151 (−2.58 %)	1649 (+1.48 %)	28.32 (+3.28 %)	0.445 (−4.51 %)	1.269 (+7.63 %)	993 (+18.07 %)
G2F0T0	161 (+3.87 %)	1617 (−0.49 %)	28.24 (+2.99 %)	0.579 (+24.25 %)	1.244 (+5.51 %)	1020 (+21.28 %)
G3F0T0	166 (+7.10 %)	1623 (−0.12 %)	30.49 (+11.20 %)	0.563 (+20.82 %)	1.260 (+6.87 %)	977 (+16.17 %)
G4F0T0	162 (+4.52 %)	1652 (+1.66 %)	29.81 (+8.72 %)	0.527 (+13.09 %)	1.183 (+0.34 %)	977 (+16.17 %)
G5F0T0	159 (+2.58 %)	1631 (+0.37 %)	31.78 (+15.90 %)	0.553 (+18.67 %)	1.314 (+11.45 %)	939 (+11.65 %)
G0F1T0	179 (+15.48 %)	1624 (−0.06 %)	29.90 (+9.04 %)	0.698 (+49.79 %)	1.438 (+21.97 %)	987 (+17.36 %)
G0F2T0	172 (+10.97 %)	1634 (+0.55 %)	30.64 (+11.74 %)	0.600 (+28.76 %)	1.373 (+16.45 %)	980 (+16.53 %)
G0F3T0	176 (+13.55 %)	1626 (+0.06 %)	31.35 (+14.33 %)	0.605 (+29.83 %)	1.293 (+9.67 %)	998 (+18.67 %)
G0F4T0	172 (+10.97 %)	1633 (+0.49 %)	31.79 (+15.94 %)	0.601 (+28.97 %)	1.287 (+6.16 %)	993 (+18.07 %)
G0F0T1	167 (+7.74 %)	1629 (+0.25 %)	28.45 (+3.76 %)	0.502 (+7.73 %)	1.213 (+2.88 %)	852 (+1.31 %)
G0F0T2	164 (+5.81 %)	1623 (−0.12 %)	29.13 (+6.24 %)	0.520 (+11.59 %)	1.382 (+17.22 %)	951 (+13.08 %)
G0F0T3	158 (+1.94 %)	1637 (+0.74 %)	29.29 (+6.28 %)	0.577 (+23.82 %)	1.490 (+26.38 %)	1016 (+20.81 %)
G0F0T4	157 (+1.29 %)	1630 (+0.31 %)	28.37 (+3.46 %)	0.629 (+34.98 %)	1.489 (+26.29 %)	1024 (+21.76 %)

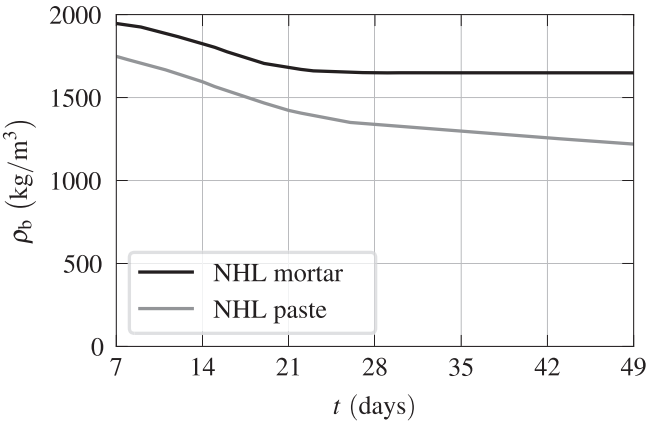

Fig. 8. Development of bulk density of unmodified NHL mortar and paste.

The development of the bulk density, ρ_b, of the unmodified NHL mortar and the NHL paste is shown in Fig. 8. All mortar types exhibited virtually identical density development. The initial decrease in density is mainly due to evaporation of free water [41]. The change in the slope of the curve indicates that hydration as per Eq. (1) mostly takes place until day 21, after which point the hardening of the mortar mostly takes place through carbonation according to Eq. (2). Carbonation resulted in an almost imperceptible increase in the density of the material at later stages of hardening. The development of the NHL paste density followed a similar pattern, with the inflection point of the curve occurring at roughly the same age. However, the density of the paste did not stabilise but continued to decrease at a slow rate until the end of the measurement period. This is possibly due to an open pore structure containing smaller diameter pores, thus prolonging the evaporation of free water in the paste specimens.

The open porosity results are visualised in Fig. 9. For G, the porosity φ tended overall to increase compared to the unmodified mortar, albeit with noticeable scatter in the results, with an increase in the filler content, with a maximum increase of 15.9 % for 20 % content. For CMF, φ tended to increase with an increase in filler content, with φ seemingly plateauing at a 15.94 % increase after 0.2 % content. Finally, for CNT, the porosity exhibited its maximum increase, equal to 6.28 %, for a content of 0.3 %. Overall increase in open porosity with an increase in filler content in cement-based mortars has been observed in similar studies employing CNT [21].

The bulk density ρ_b was not significantly affected by changes in the filler type or content, with changes ranging between −0.49 % and + 1.66 %. This is consistent with behaviour observed in cement mortars modified with CNT [4]. Coupled with the general tendency of the porosity to increase with an increase in filler content, this fact indicates that mortar modification resulted in an increase in the true density of the solid material. The changes in compressive and flexural strengths as well as modulus of elasticity of the mortars are visualised in Fig. 10. For G, the highest increase in flexural strength f_b was achieved for 2.5 % G/b (+24.25 %) while the increase in compressive strength f_c was maximum at 20 % G/b (+11.45 %). In the case of CMF, remarkable increases of + 21.97 % in f_c and + 49.79 % in f_b were achieved for only 0.01 % CMF/b. The gains in strength were reduced for higher CMF/b, tending towards roughly + 6 % for f_c and + 18 % for f_b. For CNT, the increase in f_b tended to increase almost linearly with higher filler content, with a maximum increase of + 34.98 % for 0.4 % CNT/b. However, the increase in f_c appeared to plateau at roughly + 26 % after 0.3 % CNT/b.

The increases in mortar strength, particularly those afforded by CMF and CNT, are generally more marked than those observed in cement-

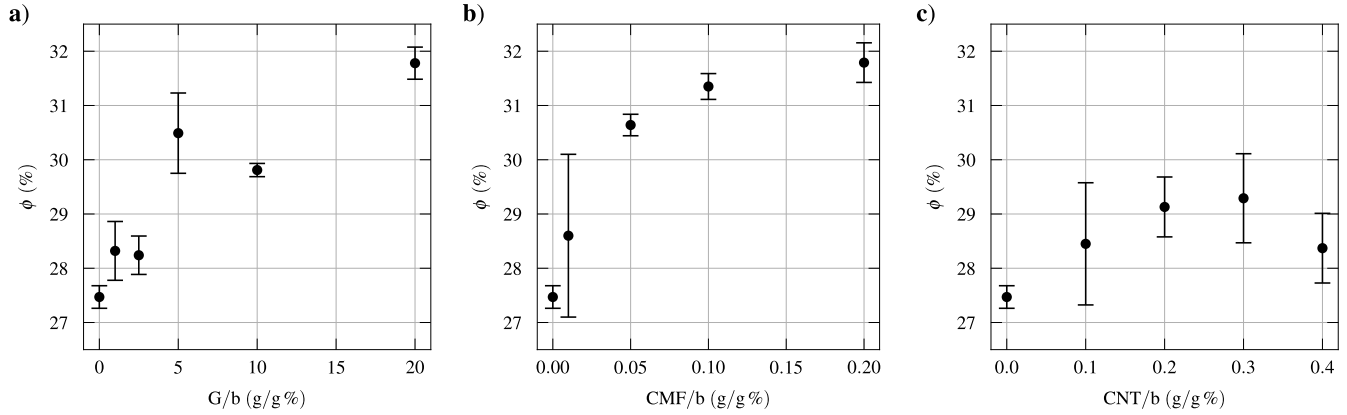

Fig. 9. Open porosity of mortar mixes for different filler content: a) G, b) CMF and c) CNT. Error bars indicate standard deviation.

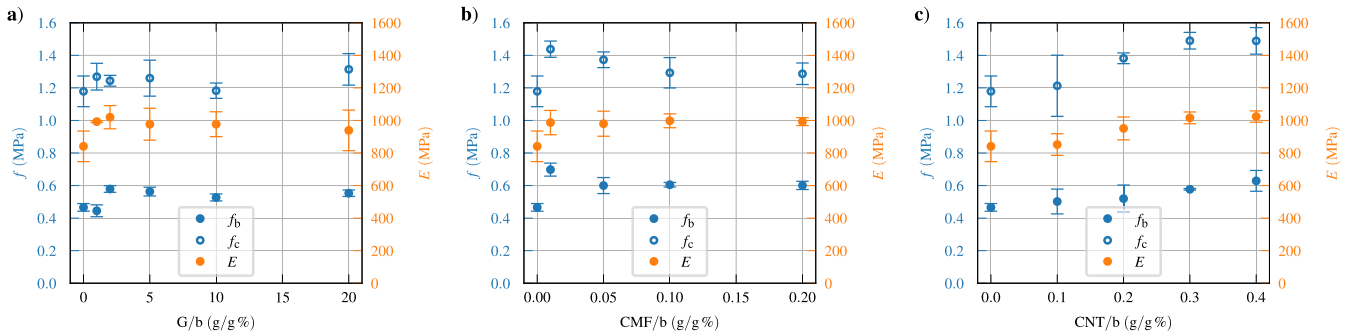

Fig. 10. Mechanical properties of mortar mixes for different filler content at the age of 49 days: a) G, b) CMF and c) CNT. Error bars indicate standard deviation.

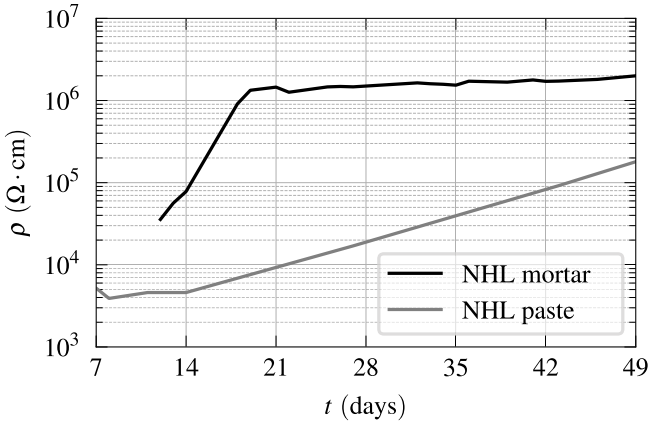

Fig. 11. Development of resistivity through time for NHL mortar and paste.

based mortars using CNT [4,21,36] but similar to the increase observed in lime-based grout modified using CNT [33]. Additionally, modification of the NHL mortar never led to a reduction of the strength, with the sole exception of a small drop in the flexural strength of the G1F0T0 mix. Finally, the Young's modulus, E, tended to increase for higher CNT/b and CMF/b up to a maximum of roughly 20 % for both fillers, as visualised in Fig. 10. In the case of G, the increase in E is maximum at 2.5 % G/b, same as for f_c. Overall, the increase in E followed a similar trend to the increase in f_c for all filler types.

The greater efficiency of CMF and CNT in enhancing the mechanical properties of the modified mortar compared to G is owed to the higher aspect ratio of the former two fillers. A higher aspect ratio enables the formation of a reinforcement net of fibres within the hardened binder that retards the formation of cracks under mechanical loading [23]. The increase in the strength and stiffness of the modified mortars, while noticeable, is not considered so excessive as to cause unwanted localised damaged in masonry walls where the material might be used. Repair mortars for historic masonry structures are expected to have similar strength and stiffness to the original mortar for ensuring compatibility and durability [1,20].

A comparison of the development of electrical resistivity, ρ, between unmodified NHL mortar and paste is illustrated in Fig. 11. The mortar displayed a rapid increase in resistivity for roughly the first 21 days, after which point the resistivity increased at a slower pace. Interestingly, the inflection point of the curve coincides with the inflection point in the density development of mortar (Fig. 8), highlighting the importance of pore moisture in electrical conductivity during the early stages of mortar hardening. Conversely, the paste exhibited an exponential increase in resistivity throughout the measurement period. The resistivity of the mortar was 1 to 2 orders of magnitude greater than the resistivity of the paste, indicating the role of aggregates and air-filled pores as electrical insulators in the mortar.

The development of the resistivity of the mortars with different filler types and content during curing is shown in Fig. 12. For all filler types and content, a rapid increase in resistivity was registered with time due to loss of moisture and, potentially, the formation of shrinkage-induced microcracks during the curing process. For the case of G, the resistivity decreased for 1 % and 2.5 % filler content, while a marked increase in resistivity for 5 % and 10 % filler content was registered at 14 days. This increase in resistivity coincided with a sudden marked drop in ambient temperature on the day of acquisition of these data. It is generally expected that a decrease in temperature can lead to an increase in the resistivity of modified cementitious materials [30]. For the case of CNTs and CMFs, the resistivity was generally reduced with an increased filler content at the early stages of hardening. Especially in the case of CMFs, an immediate substantial reduction in resistivity was registered at 0.01 % filler content. Finally, at the age of 49 days the differences in resistivity between different filler contents were reduced for all filler

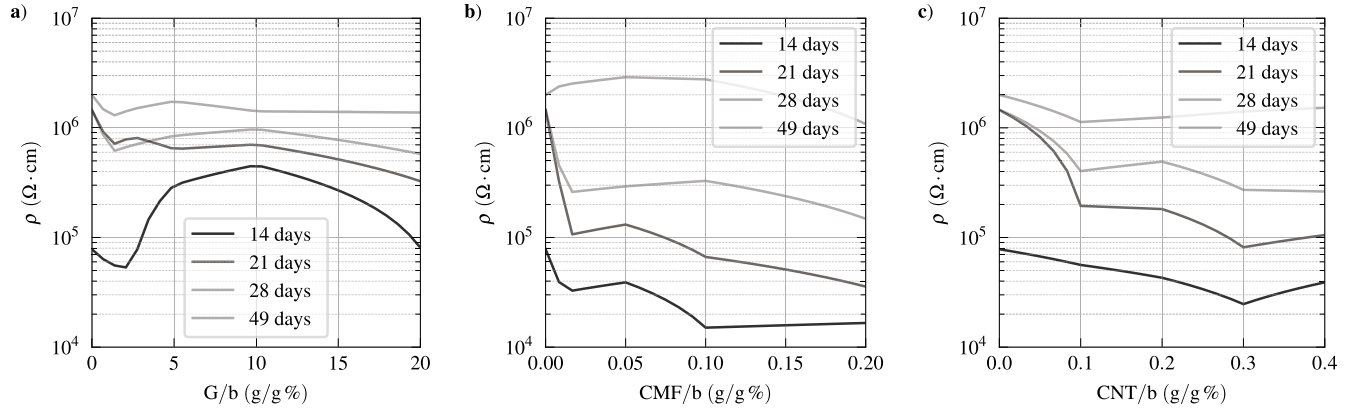

Fig. 12. Development of resistivity of mortar through time for different filler types: a) G, b) CMF and c) CNT.

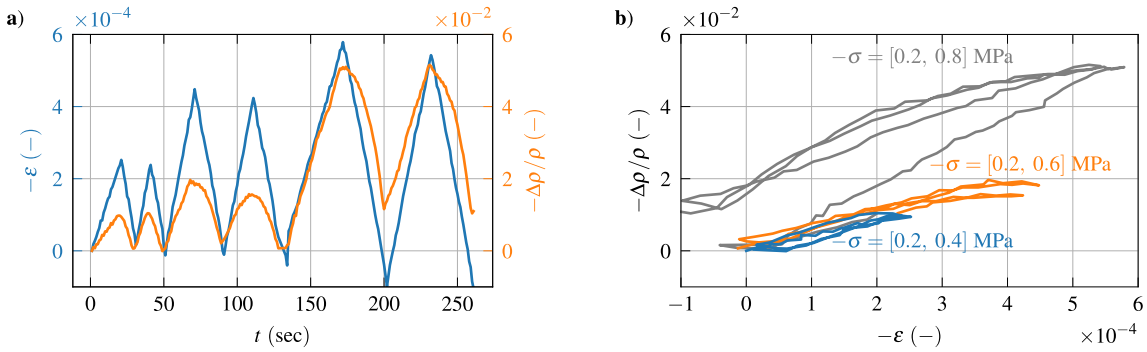

Fig. 13. Piezoresistive behaviour of G3F0T0 mortar: a) axial strain and resistivity relative change time history and b) axial strain vs resistivity relative change.

Table 7
Results of electromechanical testing for different mortar mixes (percentile difference from unmodified mortar G0F0T0 in parentheses).

Name	$\lambda(-)$	$\delta(-)$
G0F0T0	52.3	4.632×10^{-3}
G1F0T0	97.5 (+86.42 %)	2.926×10^{-3} (−36.83 %)
G2F0T0	114.3 (+118.55 %)	2.239×10^{-3} (−51.66 %)
G3F0T0	81.5 (+55.83 %)	3.079×10^{-3} (−33.53 %)
G4F0T0	146.4 (+179.92 %)	1.196×10^{-3} (−74.18 %)
G5F0T0	58.5 (+11.85 %)	4.334×10^{-3} (−6.43 %)
G0F1T0	59.4 (+13.58 %)	3.837×10^{-3} (−17.16 %)
G0F2T0	94.3 (+80.31 %)	2.472×10^{-3} (−46.63 %)
G0F3T0	133.0 (+154.30 %)	1.995×10^{-3} (−56.93 %)
G0F4T0	63.0 (+20.46 %)	4.191×10^{-3} (−9.52 %)
G0F0T1	76.5 (+46.27 %)	2.634×10^{-3} (−43.13 %)
G0F0T2	77.7 (+48.57 %)	3.549×10^{-3} (−23.28 %)
G0F0T3	61.8 (+18.16 %)	4.732×10^{-3} (+2.16 %)
G0F0T4	44.7 (−14.53 %)	5.842×10^{-3} (+26.12 %)

types.

The high content of non-conductive sand aggregates in combination with the high porosity means that the volume ratio of conductive material in the mortar, namely hardened NHL paste with or without fillers, is relatively low. Further, it means that the volume ratio of the material being modified through the fillers is also low. Hence, due to the difficulty for conductive passages to be formed [12], the relative reduction of the resistivity of the mortars resulting from modification was not as marked as in the case of paste modified with similar fillers [2]. It is, therefore, difficult to discern the percolation threshold through these results. Nevertheless, evaluation of the electromechanical test results can assist in clarifying the results of the percolation study.

An example of the time history of strain ε and relative change of resistivity $\Delta\rho/\rho$ is shown in Fig. 13a. An imposed negative (compressive) strain resulted in a decrease in resistivity. All specimens exhibited similar behaviour to the one shown. A clearer illustration of the piezoresistive behaviour of the material is shown in Fig. 13b. The cycles up to 0.4 MPa compressive stress, or roughly 33 % of the compressive strength, exhibited a linear response with good repeatability. The cycles up to 0.6 MPa, or roughly 50 % of the compressive strength, exhibited signs of small residual strain and a slightly pronounced hysteretic response. Additionally, the cycles up to 0.8 MPa, or roughly 66 % of the compressive strength, were always accompanied by residual strains and residual decrease in resistivity. Further, the specimens were damaged at the end of the tests, featuring vertical cracks due to excessive compressive loading. Therefore, it was decided to evaluate the basic piezoresistive properties of the materials using the first two loading cycles. Nevertheless, the higher stress load cycles illustrated the smart materials' capacity to detect compressive damage through residual relative resistivity changes. Assuming that the electrical properties of the bulk material were not altered after conclusion of the test, these changes in resistivity can be attributed, according to eq. (3), to a residual decrease in the effective conducting cross section A due to cracks, which was not offset by a reduction of the measurement length L due to possible residual negative strain. Therefore, resistivity measurements can be potentially used as a tool for damage detection and quantification.

The results of the electromechanical tests are summarised in Table 7. The piezoresistive sensitivity of the material is expressed through the gauge factor λ while the sensing linearity is expressed through the resolution δ equal to the 95 % confidence interval in the strain domain. Higher values for λ and lower values for δ indicate enhanced piezoresistive performance. For G, λ was maximised at roughly 10 % filler content. CMFs resulted in the maximisation of λ for a filler content of 0.1 %. Finally, for CNTs, the maximum value for λ was achieved for 0.2 % filler content.

The electromechanical test results are further shown in Fig. 14. Plotting second order polynomial regression curves for λ and δ helps in visualising the effect of modification on piezoresistive properties and in locating the filler content resulting in optimised self-sensing performance. Further, it assists in establishing that the filler content where maximisation of λ was achieved roughly coincides with the filler content for which δ was minimised, indicating the filler content where the

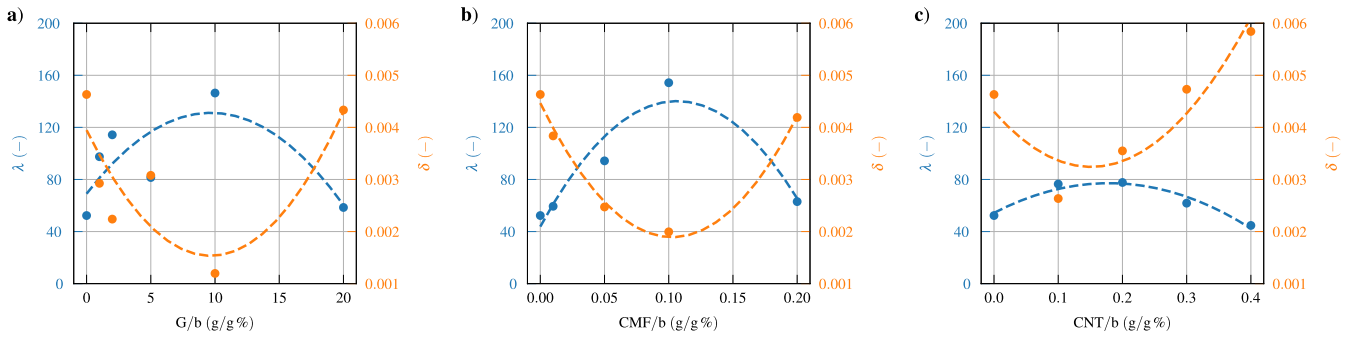

Fig. 14. Results of electrotechnical testing for different mortar mixes: a) G, b) CMF and c) CNT (second order polynomial fit curves in dashed lines).

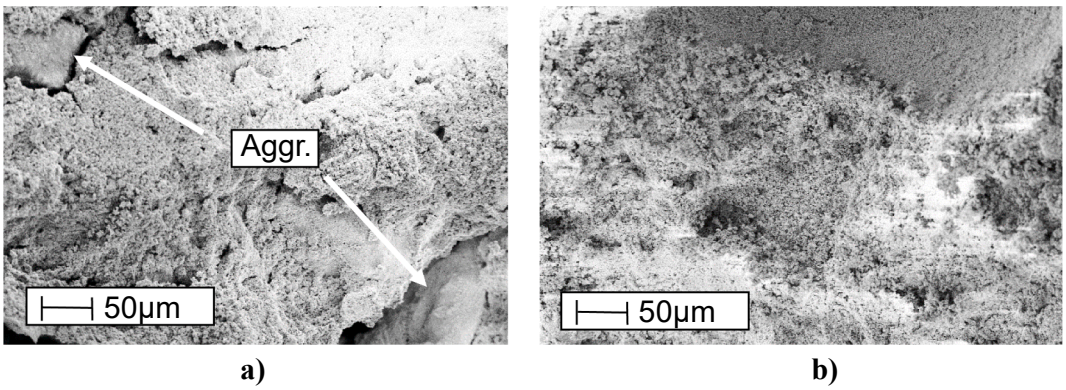

Fig. 15. SEM micrographs of a) unmodified lime mortar (aggregates indicated) and b) unmodified lime paste.

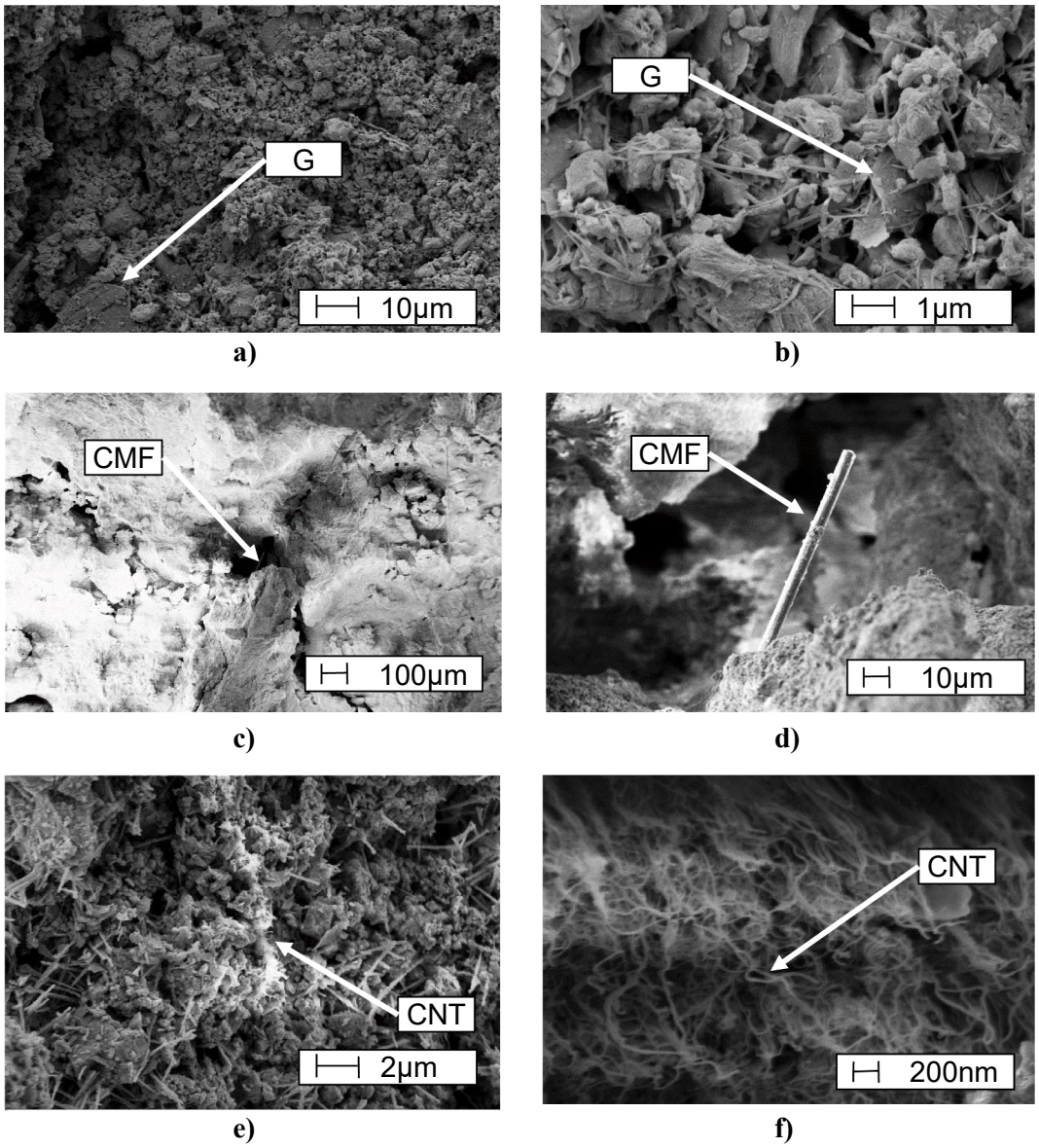

Fig. 16. SEM micrographs at different magnification levels of lime mortar doped with a) and b) 20 % G, c) and d) 0.2 % CMF, e) and f) 0.4 % CNT.

overall piezoresistive behaviour of the material is optimised. Through this observation it was established that the optimal filler contents are: ~10.0 % G, ~0.10 % CMF and ~ 0.15 % CNT. G led to the second greatest increase in λ and the highest decrease in δ but only for a high level of filler content. Piezoresistivity was optimised at roughly the same filler content for CMF and CNT, but the enhancement using CMF was

substantially greater.

Fig. 15 shows the micrographs obtained on fragments of lime mortar and paste without addition of any fillers. Both images indicate the homogeneity of the lime paste, while the mortar image indicates the discontinuity in the paste created by the presence of the aggregates. Fig. 16 shows the dispersion of CNT, G and CMF in the modified mortar at different magnification levels. While for G and CMF good dispersion is noticeable, for high doping levels of CNT the presence of some agglomerations is clearly visible.

4. Conclusions

This paper presents the mechanical and piezoresistive investigation of natural hydraulic lime mortars modified with different nano- and microscale conductive fillers. The results were evaluated in terms of enhancement of mechanical properties and self-sensing performance of the modified materials.

Graphite (G) and carbon microfibres (CMF) were characterised by ease of application, capable of being dispersed in the mortar binder through mechanical mixing, allowing their application in large quantities of mortar without the use of specialised equipment. Conversely, carbon nanotubes (CNT) require the use of sonication for filler dispersion, which is critical for higher amounts, imposing restraints on the scalability of application at the structural level.

None of the fillers had pronounced adverse effects on the workability or bulk density of the mortar, while all tended to increase its open porosity. G and CNTs caused noticeable changes in mortar colour, whereas CMFs did not cause such changes.

The greatest mechanical improvement was afforded by CMFs at a very low filler content. CNTs provided a similar percentile increase in mechanical performance but at much higher filler content. G offered a smaller degree of improvement compared to the other two fillers. None of the changes in strength and stiffness of the materials are deemed as potentially detrimental to historic masonry structures due to mechanical incompatibility.

The smart sensors can operate using alternating current of low voltage and frequency, facilitating applications in the field. G and CMFs produced the highest increase in piezoresistive sensitivity, with the former equalling this performance, coupled with the greatest improvement in linearity, although at a much higher filler content. CNTs produced only moderate piezoresistive enhancement compared to the other two fillers.

Overall, CMFs emerged as the most suitable filler for modification of lime mortar for the production of a smart intervention material targeted at historic masonry structures. A filler/binder content of 0.10 % by mass afforded substantial enhancement of mechanical performance coupled with optimised piezoresistive properties without compromising physical properties.

This investigation highlights the need for further work with multiple objectives. Additional investigation of the piezoresistive behaviour of NHL paste doped with different fillers could shed light on the percolation limits of the material. An alternative dispersion procedure for CNTs, potentially through the use of chemical dispersants and/or high energy mechanical mixing, could solve the scalability issues of this filler and provide greater piezoresistive enhancement. The use of hybrid fillers, such as G combined with CMFs, could result in improved piezoresistive behaviour with reduced total filler content. Finally, physical, mechanical and electromechanical tests of modified mortar at different ages over an extended period could provide insight into the development of the behaviour of these materials in the long term for establishing their potential as intervention materials in real applications.

CRediT authorship contribution statement

Anastasios Drougkas: Writing – original draft, Writing – review & editing, Funding acquisition, Conceptualization, Data curation, Investigation. **Vasilis Sarhosis:** Writing – original draft, Writing – review & editing, Funding acquisition, Supervision. **Muhammed Basheer:** Writing – original draft, Writing – review & editing, Funding acquisition, Supervision. **Antonella D'Alessandro:** Writing – original draft, Writing – review & editing, Methodology, Supervision. **Filippo Ubertini:** Writing – original draft, Writing – review & editing, Methodology, Supervision.

Declaration of Competing Interest

The authors declare that they have no known competing financial interests or personal relationships that could have appeared to influence the work reported in this paper.

Data availability

Data will be made available on request.

Acknowledgements

This project has received funding from the European Union's Horizon 2020 research and innovation programme under the Marie Skłodowska-Curie grant agreement No. 101023384 (S-RePaIR: Smart Restoration with Particle Infused Repointing).

The contributions of Carolina Sabatini and Dr Claudia Fabiani in the execution of the experiments are gratefully acknowledged.

References

[1] K. Van Balen, I. Papayianni, R. Van Hees, L. Binda, A. Waldum, Introduction to requirements for and functions and properties of repair mortars, Mater. Struct./Materiaux et Constructions 38 (282) (2005) 781–785, https://doi.org/10.1617/14319.

[2] H.B. Birgin, A. D'Alessandro, S. Laflamme, F. Ubertini, Hybrid carbon microfibers-graphite fillers for piezoresistive cementitious composites, Sensors (Switzerland) 21 (2) (2021) 1–13, https://doi.org/10.3390/s21020518.

[3] K. Callebaut, J. Elsen, K. Van Balen, W. Viaene, Nineteenth century hydraulic restoration mortars in the Saint Michael's Church (Leuven, Belgium): natural hydraulic lime or cement? Cem. Concr. Res. 31 (2001) 397–403.

[4] M. Camacho, O. del Carmen, F.J. Galao, E.Z. Baeza, P. Garcés, Mechanical Properties and Durability of CNT Cement Composites, Materials 7 (3) (2014) 1640–1651, https://doi.org/10.3390/ma7031640.

[5] CEN. 2005. EN-196-1 — Methods of Testing Cement — Part 1: Determination of Strength.

[6] CEN. 2007. *EN 1015-11 — Methods of Test for Mortar for Masonry — Part 11: Determination of Flexural and Compressive Strength of Hardened Mortar.*

[7] CEN. 2010a. EN 459-1 — Building Lime — Part 1: Definitions, Specifications and Conformity Criteria.

[8] CEN. 2010b. *EN 459-2 — Building Lime Part 2: Test Methods.*

[9] D.D.L. Chung, Multifunctional Cement-Based Materials, CRC Press, New York, NY, 2018.

[10] A. D'Alessandro, M. Rallini, F. Ubertini, A.L. Materazzi, J.M. Kenny, Investigations on scalable fabrication procedures for self-sensing carbon nanotube cement-matrix composites for SHM applications, Cem. Concr. Compos. 65 (2016) 200–213, https://doi.org/10.1016/j.cemconcomp.2015.11.001.

[11] A. D'Alessandro, M. Tiecco, A. Meoni, F. Ubertini, Improved strain sensing properties of cement-based sensors through enhanced carbon nanotube dispersion, Cem. Concr. Compos. 115 (2020) (2021), 103842, https://doi.org/10.1016/j.cemconcomp.2020.103842.

[12] W. Dong, W. Li, Y. Guo, Z. Sun, Q.u. Fulin, R. Liang, S.P. Shah, Application of intrinsic cement-based sensor for traffic detections of human motion and vehicle speed, Constr. Build. Mater. 355 (2022), 129130, https://doi.org/10.1016/j.conbuildmat.2022.129130.

[13] W. Dong, W. Li, K. Wang, Y. Guo, D. Sheng, S.P. Shah, Piezoresistivity enhancement of functional carbon black filled cement-based sensor using polypropylene fibre, Powder Technol. 373 (2020) 184–194, https://doi.org/10.1016/j.powtec.2020.06.029.

[14] A. Drougkas, P. Roca, C. Molins, Compressive strength and elasticity of pure lime mortar masonry, Mater. Struct. 49 (3) (2016) 983–999, https://doi.org/10.1617/s11527-015-0553-2.

[15] P. Faria, P. Duarte, D. Barbosa, I. Ferreira, New composite of natural hydraulic lime mortar with graphene oxide, Constr. Build. Mater. 156 (2017) 1150–1157, https://doi.org/10.1016/j.conbuildmat.2017.09.072.

[16] L. Fusade, S.A. Orr, C. Wood, M. O'Dowd, H. Viles, Drying response of lime-mortar joints in granite masonry after an intense rainfall and after repointing, Heritage Sci. 7 (1) (2019) 1–19, https://doi.org/10.1186/s40494-019-0277-7.

[17] L. Fusade, H.A. Viles, A Comparison of standard and realistic curing conditions of natural hydraulic lime repointing mortar for damp masonry: impact on laboratory evaluation, J. Cult. Herit. 37 (2019) 82–93, https://doi.org/10.1016/j.culher.2018.11.011.
[18] Y. Guo, W. Li, W. Dong, Z. Luo, Q.u. Fulin, F. Yang, K. Wang, Self-sensing performance of cement-based sensor with carbon black and polypropylene fibre subjected to different loading conditions, Journal of Building Engineering 59 (2022), 105003, https://doi.org/10.1016/j.jobe.2022.105003.
[19] B. Han, S. Ding, Y.u. Xun, intrinsic self-sensing concrete and structures: a review, Measurement: J. Int. Measur. Confederation 59 (2015) 110–128, https://doi.org/10.1016/j.measurement.2014.09.048.
[20] R. Van Hees, K. van Balen, B. Bicer-Simsir, L. Binda, T. von Konow, J.E. Lindqvist, P. Maurenbrecher, I. Papayanni, M. Subercaseaux, C. Tedeschi, E.E. Toumbakari, M. Thompson, J. Valek, R. Veiga, RILEM TC 203-RHM: repair mortars for historic masonry: repair mortars for historic masonry from problem to intervention: a decision process, Mater. Struct./Materiaux et Constructions 45 (9) (2012) 1295–1302, https://doi.org/10.1617/s11527-012-9917-z.
[21] S. Hu, X.u. Yaoqun, J. Wang, P. Zhang, J. Guo, Modification effects of carbon nanotube dispersion on the mechanical properties, pore structure, and microstructure of cement mortar, Materials 13 (5) (2020), https://doi.org/10.3390/ma13051101.
[22] V.M. Karbhari, L.S.W. Lee, 6 - Vibration-Based Damage Detection Techniques for Structural Health Monitoring of Civil Infrastructure Systems, in: V.M. Karbhari, F. Ansari (Eds.), *Structural Health Monitoring of Civil Infrastructure Systems, Woodhead Publishing Series in Civil and Structural Engineering*, Woodhead Publishing, 2009, pp. 177–212.
[23] M.S. Konsta-Gdoutos, G. Batis, P.A. Danoglidis, A.K. Zacharopoulou, E. K. Zacharopoulou, M.G. Falara, S.P. Shah, Effect of CNT and CNF loading and count on the corrosion resistance, conductivity and mechanical properties of nanomodified OPC mortars, Constr. Build. Mater. 147 (2017) 48–57, https://doi.org/10.1016/j.conbuildmat.2017.04.112.
[24] J. Lanas, J.I. Alvarez-Galindo, Masonry repair lime-based mortars: factors affecting the mechanical behavior, Cem. Concr. Res. 33 (11) (2003) 1867–1876, https://doi.org/10.1016/S0008-8846(03)00210-2.
[25] J. Lanas, J.L. Pérez Bernal, M.A. Bello, José I. Alvarez-Galindo., Mechanical properties of masonry repair dolomitic lime-based mortars, Cem. Concr. Res. 36 (5) (2006) 951–960, https://doi.org/10.1016/j.cemconres.2005.10.004.
[26] W. Li, Q.u. Fulin, W. Dong, G. Mishra, S.P. Shah, A comprehensive review on self-sensing graphene/cementitious composites: a pathway toward next-generation smart concrete, Constr. Build. Mater. 331 (2022), 127284, https://doi.org/10.1016/j.conbuildmat.2022.127284.
[27] N. Makoond, A. Cabané, L. Pelà, C. Molins, Relationship between the static and dynamic elastic modulus of brick masonry constituents, Constr. Build. Mater. 259 (2020), 120386, https://doi.org/10.1016/j.conbuildmat.2020.120386.
[28] D. Marastoni, L. Pelà, A. Benedetti, P. Roca, Combining Brazilian tests on masonry cores and double punch tests for the mechanical characterization of historical mortars, Constr. Build. Mater. 112 (2016) 112–127, https://doi.org/10.1016/j.conbuildmat.2016.02.168.
[29] P. Maravelaki-Kalaitzaki, A. Bakolas, I. Karatasios, V. Kilikoglou, Hydraulic lime mortars for the restoration of historic masonry in crete, Cem. Concr. Res. 35 (8) (2005) 1577–1586, https://doi.org/10.1016/j.cemconres.2004.09.001.
[30] A. Meoni, A. D'Alessandro, M. Mancinelli, F. Ubertini, A multichannel strain measurement technique for nanomodified smart cement-based sensors in reinforced concrete structures, Sensors 21 (16) (2021), https://doi.org/10.3390/s21165633.
[31] S. Pavía, R. Hanley, Flexural bond strength of natural hydraulic lime mortar and clay brick, Mater. Struct./Materiaux et Constructions 43 (7) (2010) 913–922, https://doi.org/10.1617/s11527-009-9555-2.
[32] G.T. Pham, Y.-B. Park, Z. Liang, C. Zhang, B. Wang, Processing and modeling of conductive thermoplastic/carbon nanotube films for strain sensing, Compos. B Eng. 39 (1) (2008) 209–216, https://doi.org/10.1016/j.compositesb.2007.02.024.
[33] L. Restuccia, A. Lopez, G.A. Ferro, D. Liberatore, J.M. Tulliani, An investigation of the beneficial effects of adding carbon nanotubes to standard injection grout, Fatigue Fract. Eng. Mater. Struct. 41 (1) (2018) 119–128, https://doi.org/10.1111/ffe.12663.
[34] S. Scannell, M. Lawrence, P. Walker, Impact of aggregate type on air lime mortar properties, Energy Procedia 62 (2014) 81–90, https://doi.org/10.1016/j.egypro.2014.12.369.
[35] J. Segura, L. Pelà, P. Roca, Monotonic and cyclic testing of clay brick and lime mortar masonry in compression, Constr. Build. Mater. 193 (2018) 453–466, https://doi.org/10.1016/j.conbuildmat.2018.10.198.
[36] P. Sikora, M.A. Elrahman, D. Stephan, The influence of nanomaterials on the thermal resistance of cement-based composites—a review, Nanomaterials 8 (7) (2018) 1–33, https://doi.org/10.3390/nano8070465.
[37] G. Song, C. Wang, B.o. Wang, Structural Health Monitoring (SHM) of civil structures, Appl. Sci. 7 (8) (2017), https://doi.org/10.3390/app7080789.
[38] S. Sony, S. Laventure, A. Sadhu, A literature review of next-generation smart sensing technology in structural health monitoring, Struct. Control Health Monit. 26 (3) (2019), e2321, https://doi.org/10.1002/stc.2321.
[39] Ubertini, Filippo, and Antonella D'Alessandro. 2018. '18 - Concrete with Self-Sensing Properties'. Pp. 501–30 in *Eco-Efficient Repair and Rehabilitation of Concrete Infrastructures*, *Woodhead Publishing Series in Civil and Structural Engineering*, edited by F. Pacheco-Torgal, R. E. Melchers, X. Shi, N. De Belie, K. Van Tittelboom, and A. Sáez. Woodhead Publishing.
[40] E. Verstrynge, L. Schueremans, D. Van Gemert, Time-dependent mechanical behavior of lime-mortar masonry, Mater. Struct. 44 (1) (2011) 29–42, https://doi.org/10.1617/s11527-010-9606-8.
[41] D. Zhang, J. Zhao, D. Wang, X.u. Chenyang, M. Zhai, X. Ma, Comparative study on the properties of three hydraulic lime mortar systems: natural hydraulic lime mortar, cement-aerial lime-based mortar and slag-aerial lime-based mortar, Constr. Build. Mater. 186 (2018) 42–52, https://doi.org/10.1016/j.conbuildmat.2018.07.053.